Seismic response of steep slopes inferred from ambient noise and accelerometer recordings: the case of Dadu River valley, China

Del Gaudio Vincenzo[a,b,*], Zhao Bo[b], Luo Yonghong[b], Wang Yunsheng[b], Wasowski Janusz[c,*]

[a] Dipartimento di Scienze della Terra e Geoambientali, Università degli Studi di Bari "Aldo Moro", Italy
[b] State Key Laboratory of Geo-Hazard Prevention and Geo-Environment Protection, Chengdu University of Technology, P.R. China.
[c] Consiglio Nazionale delle Ricerche – Istituto di Ricerca per la Protezione Idrogeologica, Bari, Italy
* Corresponding author.

ABSTRACT

Seismic site effects (local topographic / lithologic amplification, directivity phenomena) can have substantial impact on slope dynamic response and susceptibility to earthquake-induced failures. However, the instrumental data needed to quantify the site effects on slopes are still scarce. Here we investigate dynamic response of steep slopes in the Dadu River valley (Sichuan Province), one of the China's regions most struck by large magnitude earthquakes. We analyse ambient noise recordings acquired at the sites of a local accelerometer network established few years after the 2008 Wenchuan earthquake. The analysis benefits from the application of a new technique that determines the ellipticity of Rayleigh waves present in noise wavefield from the instantaneous polarization analysis of the recorded signals. The technique is adapted for application to steep surface by rotating the noise recordings according to a reference having as axes the slope down-dip direction, the slope surface strike and the normal to the slope surface. This allows obtaining the curve of Rayleigh wave ellipticity as function of frequency, whose maxima provide information on site response characteristics, and leads to a more reliable identification of resonance phenomena on steep slopes (40° inclination). The results of the ambient noise analysis are consistent with the available accelerometer data and provide clear indication of significant resonance effects, with regard to their potential impact on local seismic slope stability. In particular, the slopes around the confluence of a local torrent with the Dadu River near the Lengzhuguan village exhibit strong site amplifications related to the presence of surficial deposits overlying intensely fractured granite bedrock. The frequency, amplitude and direction of resonance phenomena derived from the analysis of instrumental data indicate that site amplification is likely to have lesser impact on the stability of the lower part of the Mt. Dagang, which forms a long steep sub-planar slope facing the Dadu River. Our findings demonstrate that expeditious ambient noise recordings can provide useful information on relative susceptibility of slopes to seismically induced failures.

Keywords: Seismic response; slope stability; ambient noise analysis; accelerometer data; Rayleigh waves; Lengzhuguan – Sichuan – China.

Published on Engineering Geology, doi: 10.1016/j.enggeo.2019.105197

1. Introduction

The 2008 M_w 7.9 Wenchuan earthquake has prompted many new studies on collateral seismic hazards in China. This has resulted in hundreds of papers on topics ranging from the spatial patterns of co-seismic landsliding to slope failure triggering and landslide runout mechanisms, the generation and failure of landslide dams, the enhanced post-seismic mass wasting and landscape evolution (e.g., Fan et al. 2018).

However, relatively few works have focused on detailed-scale characterization of slope dynamic response based on accelerometer monitoring (e.g., Luo et al., 2013, 2014; Wang et al., 2015, 2017; Del Gaudio et al., 2018). Indeed, such studies typically require the availability of important funds for setting up and maintaining local accelerometer networks, as well as temporally extensive (years) monitoring periods to acquire a significant number of earthquake recordings.

As emphasized by Wasowski et al. (2011), there is a general need to acquire more seismic recordings from accelerometer stations located on slopes. This stems from the observational and instrumental evidence that slopes can be influenced by pronounced seismic site effects (local topographic / lithologic amplification, directivity phenomena), which can have substantial impact on their dynamic response and susceptibility to earthquake induced failures (e.g., Del Gaudio and Wasowski, 2011; Moore et al., 2011; Burjanek et al., 2014; 2018; Kleinbrod et al., 2019). Therefore, more strong motion data recorded on slopes of interest are required to provide realistic inputs for modelling slope dynamic behavior and constraining seismic landslide hazard assessment.

Regarding the mountainous area (Longmenshan) struck by the 2008 Wenchuan earthquake, one of the first local accelerometer monitoring systems was set up on the peri-urban slopes in the town of Qiaozhuang (Qingchuan County) located about 250 km NE of the mainshock epicentre (Fig. 1). The town is near the NE termination of the active Yingxiu-Beichuan fault and a number of accelerometer stations registered aftershocks of the Wenchuan sequence as well as other seismic events (Luo et al., 2014). The direct information on slope seismic response obtained from accelerometer recordings, as well as repeated ambient noise measurements (Luo et al., 2014; Del Gaudio et al., 2018), provided evidence of the combined influence of local topography and geology on the site amplification and directivity phenomena. The site effects were present, in particular, in the uppermost parts of local reliefs made of fractured limestones and phyllites. However, the exact influence of topographic and geologic features on the slope seismic response remained uncertain.

Within the above context, we present new data on dynamic response of slopes in a high mountain area of southwestern China located in the Dadu River watershed (Sichuan Province, Fig. 1). With its length exceeding 1000 km, the Dadu River represents one of the most important watercourses draining the eastern margin of the Tibet Plateau. This area is located near the junction of two major tectonic shear zones: the NW-SE trending Xiannshuhe fault zone and NE-SW Longmenshan fault zones (Fig. 1). It is one of the most seismically active regions of China, as demonstrated by the recurrence of large magnitude (M>7) earthquakes (Allen et al., 1991; Chen et al., 2012). The Neogene tectonic activity (with its current phase that started in late Pliocene-Pleistocene) is responsible for the presence of very high relief mountainous terrain (elevations exceeding 6000 m) and high erosion rates (Xu and Kamp, 2000). Steep valley slopes, frequent seismic events and river erosion are important factors of landsliding in the Dadu River watershed (e.g., Dai et al., 2005; Deng et al., 2017).

The high rates of tectonic and geomorphic activity motivated the establishment of several accelerometer stations on the valley slopes near the Lengzhuguan village, located in the middle reaches of the Dadu River, less than 20 km NNW from the town of Luding (Figs. 1, 2). Several stations were also positioned up to 240 meters inside the rocky slope in an abandoned water tunnel (Fig. 3d-e), which in the past was used for hydropower generation. This and the presence of steep slopes (≥ 40°) make the Lengzhuguan study area rather unique among the few hillslope test sites in the world with ongoing long-term accelerometer monitoring.

Research on seismic response of slopes at Lengzhuguan is important, as there is evidence that the Dadu River damming by earthquake-triggered slope failures can have disastrous consequences on the population living in the river valley. This was well demonstrated by Dai et al. (2005), who used historic and geomorphic data to reconstruct the formation of a large landslide dam triggered by the 1786 M7.8 earthquake and subsequent dam-breach and catastrophic flood (over 100,000 deaths). Assessment of slope failure and landslide damming hazards is also relevant to the management of the major hydropower projects that have recently been developed in the Dadu River valley (Tu et al., 2018).

The accelerometers were set up at Lengzhuguan few years after the 2008 Wenchuan event, and recorded the mainshock of the 2013 Lushan earthquake (Ms 7.0) and the two major shocks of the 2014 Kangding seismic sequence, which occurred on 22 and 25 November with magnitude Ms 6.2 and 5.8, respectively (China Earthquake Database, CNEC, http://earthquake.cn). The accelerometer records from this and earlier smaller magnitude seismic events provided information for the initial assessment of dynamic response of slopes near Lengzhuguan (Luo et al., 2013; Wang et al., 2015, 2017).

In consideration of the limited amount of data acquired until now by the Lengzhuguan accelerometer stations, here we expand on the above-mentioned earlier works by using a series of complementary ambient noise recordings conducted in 2017 and 2018. While the earlier studies assumed the presence of uniform lithologic conditions (moderately to slightly weathered Proterozoic granite) and emphasized the influence of topographic factor on seismic slope response, we provide more focus on the local geology and especially on the presence of surficial deposits that mantle the steep slopes in granitic rocks at Lengzhuguan. This and the combined use of accelerometer and ambient noise recordings leads to a more constrained interpretation of seismic response of slopes. We show that the variations in site response in terms of site amplification reflect local changes in slope geology (in particular, changes in impedance contrast and thickness of the surficial materials overlying the fractured granites), whereas the directivity effects seem to depend on the combined influence of the local topographic and structural setting.

2. Geological setting

The study area is located in Luding County, at the confluence of the Lengzhuguan Torrent to the Dadu River (Figs. 1, 2). Very high mountains and deeply incised river valleys dominate the landscape in this part of Sichuan. In the immediate vicinity of the study area, the elevation ranges from about 1350 m a.s.l. (river valley bottom) to over 3000 m (valley slopes). However, within less than 12 km distance to SSW (toward the town of Kangding), the elevations exceed 5800 m a.s.l. (Fig. 1).

2.1 Geomorphic and geologic features

Local slopes have high topographic gradient (Figs. 2 and 3), supported by the presence of bedrock consisting of moderately to slightly weathered Proterozoic granites (Luo et al., 2013; Wang et al., 2015: Fig. 4). Overall, the inclinations of the investigated slopes are around 40°. Field observations and topographic profiles (P2 and P4, Figs. 2-3) indicated the presence of a slope break and steeper topography on the Mt. Dagang hillslope facing the Dadu River (east facing), about 600-700 m above the river level (Fig. 5). This feature is about 100 m high and can be interpreted as a degraded scarp of a presumably deep-seated old landslide. The toe of the slope coincides with a sharp bend in the Dadu River, where we can expect enhanced erosion rates. The original landslide material might be gone by now, or we failed to distinguished it from the bedrock, considering the ubiquitous presence of fractured rocks. The slope is mantled by variable thickness (from few to about 10 m thick), surficial deposits within which a number of distinct landslide bodies can be recognized (likely of rockfall, debris flow/avalanche and rockslide origin). Significantly, moving away (northward and southward) from the inferred failed slope, the topographic gradient increases (> 40°, e.g., profile 3 in Figs. 2-3). The geomorphic features of the topographically much lower, NE-facing slopes of Mt. Huoshao provide clearer evidence of apparently more recent failures along the erosive bend of the Dadu River

(Fig. 2). A concave-convex morphology can be recognized (profile 1 in Fig. 3), and our in situ inspection confirmed the presence of a scarp (upper slope) and of a landslide deposit with many rock blocks in the middle-lower slope (Fig. 4a). The upper-most part of the relief is flat. This and the presence of a colluvial deposit and some alluvial material (sub-rounded clasts) could be indicative of the remnant of a river terrace.

2.2 Landslide triggers and relative seismic slope susceptibility

Although the geomorphic forms and field evidence point to recurrent landsliding in the study area, documented examples of earthquake- or rainfall-triggered slope failures are lacking for Lengzhuguan. Indeed, the area is scarcely populated and historical records seem very limited. Nevertheless, the importance of seismic landslide triggering has been clearly demonstrated by the studies conducted elsewhere in the Dadu River valley, e.g., in the Luding County (Dai et al., 2005; Deng et al., 2017).

Precipitation data are not available for the Lengzhuguan area. Nevertheless, in the neighboring county to the north (Danba County), the average annual rainfall is 600 mm (Fei et al., 2012), while it reaches 637 mm at Luding located less than 20 km to the south (Dai et al., 2005). Most of this rainfall occurs in the summer months when the river's discharge (with its erosive power) reaches its maximum. Therefore, we suspect that slope failures are likely to occur in the wet season.

In general, it is recognized that steep rock slopes characterized by the presence of open fractures are highly susceptible to earthquake-induced failure (e.g., Keefer, 1993; Harp and Noble, 1993). Therefore, we can assign relatively high seismic failure susceptibility to the rock slopes at Lengzhuguan. The presence of open fractures and shattered bedrock can be linked to the large magnitude earthquakes that have struck the area in the last few centuries.

2.3 Site setting of the accelerometer stations

Considering the in situ evidence, the setting of the accelerometer stations (Figs. 2, 3, 4) can be summarized as follows:

Station L1 – relatively flat, hilltop of a ridge elongated in NNE direction; up to several meter thick surficial deposits overlying a shattered bedrock (open fractures);

Station L2 – NE termination of the above-mentioned ridge, at the middle-lower part of a landslide scarp (NE facing slope); up to few meter thick chaotic deposit (boulders and large blocks) overlying a shattered bedrock;

Station L3 – at slope base, granitic bedrock, fractures (mostly closed); at the west bank of the Lengzhuguan Torrent;

Station L4 – lower part of the slope, close to a convex slope break near the rim of the Lengzhuguan Torrent gorge; local colluvium/landslide deposit, up to few meter thick, overlying granitic bedrock (not outcropping);

Station L5 – comparable to L4, but more pronounced convex slope break with very steep topography (Lengzhuguan Torrent gorge); larger and unstable secondary landslide deposit (open fractures), with estimated thickness ranging from several to perhaps more than 10 meters, overlying shattered granitic bedrock (open fractures), irregular bedrock topography;

Station L6 – lower part of the large failed slope (near the left flank of the old landslide), nearly planar slope, secondary creeping landslide (open fractures), several or more meters thick;

Station L7 – middle part of the large failed slope (near the left flank of the old landslide), nearly planar slope, shattered bedrock (open fractures) or secondary rockslide deposit.

3. Data acquisition and analysis methodologies

In order to investigate the dynamic response of slopes in the Lengzhuguan area, we acquired ambient noise recordings during three campaigns, the first in June 2017, the second in late October of the same year and the third in late October 2018. We used three tromographs Tromino, compact 3-component electrodynamic velocimeters, specifically designed to record small amplitude ground vibrations (see http://moho.world/en/tromino/ for details).

During the first campaign, two tromographs were used to acquire 30 minute noise recordings at the sites of accelerometer stations L1, L2, L3, L4 and L5, located on the opposite sides of the Lengzhuguan Torrent gully, and inside the tunnel located at site L7 on the Mount Dagang slope facing the Dadu River (Figs. 2, 3). In particular, the measurements were carried out near the tunnel entrance (site named L7), and at the sites of five of the accelerometer stations inside the tunnel, i.e., L7-1, L7-3, L7-4, L7-6 and L7-7 (Fig. 3-e).

During the second campaign (October 2017), one tromograph was kept continuously recording at site L7. Based on the results of our initial analyses, this site was found to be only little affected by amplification and, therefore, used as reference to check possible variation of noise wavefield during the two-day measurements and between different campaigns (cf. Del Gaudio et al., 2014). At the reference station, noise was recorded for several hours during each measurement day. The other tromograph was deployed for 30 minute recording sessions at the sites investigated in the previous campaign. Additional measurements were carried out on the Mount Dagang slope, in front of the entrance of another water tunnel (site L6), located about 130 m below L7, and at the sites of two additional accelerometer stations inside the tunnel L7, skipped in the previous campaign (L7-2 and L7-5 in Fig. 3-e).

In the third campaign (October 2018), three tromographs were employed to repeat measurements at selected sites. The site L7 near the entrance of the upper tunnel was again adopted as reference, acquiring continuous noise recordings, whereas shorter recording sessions, generally of 30 minutes, were carried out at sites L5, L6 and at the sites of all the accelerometer stations inside the L7 tunnel.

Noise recordings were analysed using both the standard Nakamura's (1989) technique, based on the calculation of spectral ratio between horizontal and vertical component of noise recording (hereinafter referred to as HVNR) and the new technique HVIP (Horizontal to Vertical ratio from Instantaneous Polarization analysis: see Del Gaudio, 2017).

The Nakamura's method was applied following the guidelines recommended by the project SESAME (Site EffectS assessment using AMbient Excitations: Bard and the SESAME Team, 2004). Ratios H/V between spectral amplitudes of horizontal and vertical components of noise recordings were averaged over several tens of 20-second time windows, after removing those showing H/V values strongly different from the average.

The HVIP method analyses the instantaneous polarization properties of a three-component recording $\overrightarrow{u(t)}$ of ambient noise through the analytic transformation

$$\overrightarrow{u_c}(t) = \overrightarrow{u(t)} + j\overrightarrow{\hat{u}(t)} \quad (1)$$

where j is the imaginary unit and $\hat{u}(t)$ is the Hilbert transform of $u(t)$. It can be demonstrated that the vector $\overrightarrow{A(t)}$ describes in real space elliptical trajectories whose principal axes change instant by instant and can be derived from the analytic signal (1) (Morozov and Smithson, 1996). Thus, this analysis allows identifying wave packets with a coherent polarization of Rayleigh type, i.e. characterised by an elliptical particle motion lying on a sub-vertical plane and having principal axes in approximately horizontal and vertical direction. The same kind of transformation (1), if applied to the two horizontal components of $\overrightarrow{u(t)}$, allows identifying, instant by instant, direction and amplitude of maximum horizontal ground motion H_{max}, whereas, applied separately to the vertical component, gives an instantaneous estimate of the amplitude V of its envelope.

This kind of analysis is carried out on recordings filtered through Gaussian filters with different central frequency f_c. Averaging the instantaneous estimates of ratios H_{max}/V only for wave packets identified as Rayleigh waves, one can obtain an estimate of their ellipticity as function of frequency f_c and also examine ellipticity variations with polarization direction. This approach is motivated by the observation that the variation of Rayleigh wave ellipticity with frequency shows peak values at site resonance frequencies: the amplitude of such peaks (i.e. the relative maxima of the *Hmax* /*V* ratios) is correlated to the amplification factor and directional variations can reveal the occurrence of site response directivity (cf., Del Gaudio et al., 2014).

The amplitudes of ellipticity peaks can provide more stable and reliable information on the amplification factors than the amplitudes of HVNR peaks (i.e., the relative maxima of H/V spectral ratios). Indeed, the latter can vary from one measurement to another, depending on the proportion of different waves present in ambient noise (Love waves, P and S waves) mixed with Rayleigh waves and which differently contribute to the amplitude of H and V components of ground motion.

4. Results

4.1 Sites L1-L2 (Mt. Huoshao)

The local setting of these two measurement sites is illustrated in Figs. 2, 3 and 4. One station (L1) is located at the top of the hill, whereas the second one (L2) is about 40 m below.

Noise data, analysed using both the HVNR and HVIP techniques, show consistent evidence of site resonance at frequencies around 3 Hz (Fig. 6). HVNR provides sharper peaks in H/V spectral ratios (H/V = 7.2 at 3.45 Hz in June 2017 and 8.1 at 2.85 Hz in October 2017 - Fig. 7a) having a more directional character, with an approximately ESE directed maximum exceeding the orthogonal minimum by 44% and 68% in June and October, respectively.

An overall inspection of polar diagrams (Fig. 6) and HVIP curves along directions of significant maxima (Fig. 7a), suggests a more complex composition of the resonance peaks, with a possible overlap of more maxima with different directions between 2 and 4 Hz. This could be related to a geomorphic complexity of the relief shape with varying orientation of the crest lines (Fig. 2), the presence of the alluvial/colluvial “terrace” (L1 - Fig 4a) and landslide deposits (L2 – Fig. 4b) overlying a shattered granitic bedrock.

With regard to L2 site, the results of the HVNR analysis of the June 2017 campaign data (Fig. 6, 7b) appear contaminated by some anomalous signals producing strong narrow peaks with decreasing amplitude at a series of four frequencies (0.5, 1.0, 1.5, 2.0 Hz). They are apparently artificial signals of uncertain origin and transitory nature, being absent in the October 2017 measurements, when a main peak with amplitude 4.3 at 2.3 Hz was observed along the azimuth N15°E. A careful inspection of the H/V diagrams shows that this peak is also present in June 2017 measurements, but almost hidden by the 2.0 Hz artificial peak (Fig. 7b).

It is noteworthy that, with respect to HVNR, the artificial signals have a much lower effect on the outcome of the HVIP analysis, possibly because they are largely filtered out due to a limited content of Rayleigh waves. Indeed, in HVIP values derived from June measurements, the artificial signals at 0.5, 1.0 and 1.5 Hz appear as secondary peaks with greatly reduced amplitudes and the peak at 2.0 Hz appears englobed within the absolute maximum at 2.25 Hz. This frequency coincides with that of the peak recognizable from the HVNR analysis and also with one of the peaks forming the complex HVIP/HVNR maxima observed at L1 site, with which it shares the same direction (N25°E). Such a similarity suggests a common origin of this peak at L1 and L2 sites. This can be related to structural factors and to a velocity contrast present at greater depth than those responsible for higher frequency maxima (e.g., the secondary peaks observed at L1 around 3-4 Hz and those found at L2 around 8 and 10 Hz).

The Rayleigh wave ellipticity curves do not provide constraints for a univocal modelling of subsoil velocity. However, simple inversions constrained by the geological observations can provide some indications about velocity models. Using the open source package dinver, produced within the geopsy project (www.geopsy.org) and based on an effective algorithm of forward modelling (Wathelet, 2008), we obtained schematic models that are compatible with the average ellipticity curves obtained at L1 and L2 during the two campaigns. The models include three layers with similar velocities for both sites, i.e., a thin surface layer with shear-wave velocity Vs ≈150 m/s (~5 and 3 m thick at L1 and L2, respectively) overlying a stiffer 15-20 m thick rock with Vs around 400 m/s and a deeper bedrock with Vs around 850 m/s. The three-layer model seems to fit the surface deposits (alluvial/colluvial "terrace" at L1 and landslide debris at L2) overlying the weathered/intensely fractured granite, which at depth is followed by more compact granitic rock.

4.2 Sites L3-L4-L5 (Mt. Dagang, NW side of the Lengzhuguan gully)

The stations L3, L4 and L5 are located at increasing elevations, with L3 positioned near the bottom of the gully, and L5 located about 100 m above (Figs. 2, 3). Measurements at L5 were carried out at two different locations, one near the accelerometer station positioned inside a horizontal shaft excavated in the slope, and the other, named L5b, positioned about 15 m from the shaft entrance.

Evidence of resonance at L5 can be recognized from the outcomes of the first campaign (see the two top-left diagrams in Fig. 8). The resonance is more clear in the results of the HVIP analysis, which show a pronounced NE directed peak (H/V= 4.4) at 5.1 Hz, whereas the HVNR analysis gives a lower maximum (H/V=3.4) at a frequency of 6 Hz in N15°E direction (see also Figure 9a).

In October 2017, the measurements were repeated deploying the tromograph outside the shaft (L5b). within about 15 m from L5. The results showed a major peak at a higher frequency in comparison to the previous measurements (H/V=5.2 at 8.25 Hz). The different positioning of the tromograph in the two recordings left an uncertainty about whether the difference in the results was due to the occurrence of an occasional disturbance in the noise wavefield, or reflected a spatial variation of site effect related to the local geology. Therefore, measurements were repeated in October 2018 using two tromographs to obtain simultaneous recordings at L5 and L5b sites. The new data showed a good consistency among the measurements acquired at the same position (see Fig. 9a-b), and confirmed the differences in site response at L5 and L5b, despite their very close location. This shows that site response can vary within a short distance, because of significant changes in local geology. In this case, we likely recorded the effect of thickness variation of secondary landslide deposits mantling the bedrock at L5 and L5b, with the maximum of amplification showing higher frequencies where the thickness of the deposits is smaller (less than 10 m).

The main resonance frequency f_0 of a site, resulting from the velocity contrast between a surface (soft) deposit and a stiffer bedrock can be approximately related to the velocity Vs and thickness h of the surface layer through the formula $f_0=Vs/4h$. Thus, assuming the landslide deposits at L5 – L5b sites have a Vs similar to that at Mt Huoshao sites, i.e., around 150-200 m/s, the increase of maximum resonance frequency from 5 to 8 Hz could result from a decrease in thickness of surface deposit by 60%, e.g., from 7-10 m to 4-6 m.

The measurements at the station L4 provided evidence of directional resonance at even higher frequencies (Fig. 8). The HVIP analysis of the June 2017 measurements revealed two major peaks at 13.85 Hz (H/V=4.6) in N75°E direction and at 17.35 Hz (H/V=3.7) in N45°E direction. These results were substantially confirmed by October 2017 measurements, apart from a 20% increase of the second peak amplitude (H/V=4.5 at 13.75 Hz in N65°E direction and H/V=4.6 at 17.85 Hz in N35°E direction). The outcome of the HVNR analysis also indicated the presence of these two peaks. Such high resonance frequencies can be attributed to the effect of thin surface deposits, which, following the same approximations adopted for L5 - L5b sites, should have a thickness of the order of 2 – 4 m.

With regard to the station L3, at the bottom of the gully, the analysis of data did not provide convincing evidence of significant site resonance. No clear peak emerges from the HVIP curves of the two campaigns (Fig. 9c). The polar diagrams (Fig. 8, bottom-right) showed relatively high levels of ellipticity (H/V>3) in the directions between N65°E and N85°E. However, from one measurement to the other, none of these peaks showed persistent frequency properties that could be related to site-specific response. The variability of the H/V curves suggests a possible influence of variations in noise wavefield generation, which can be linked to the site closeness (within 15 m) to the torrent. This makes the recording conditions particularly noisy.

4.3 Sites L6-L7 (Mount Dagang slope facing the Dadu River)

A peculiarity of sites L6 and L7 is their location on a long sub-planar part of more than two km long steep (about 40°) slope (Figs. 4, 5). This setting poses some problems to the processing of ambient noise, which is commonly assumed to consist mainly of surface waves (cf. Bonnefoy-Claudet et al., 2006). In particular, if the interpretation is focused on properties of Rayleigh waves, the assumption that the ratios between horizontal and vertical component of ground motion provide a measurement of Rayleigh wave ellipticity may not be fully justified. On steeply inclined slope, especially for wavelengths significantly shorter than the slope length, the ellipse axes of Rayleigh wave particle motion are expected to assume orientations parallel/normal to the slope surface rather than in horizontal/vertical directions.

Based on these considerations, we tested an approach to adapt the HVIP technique to such a steep slope. This consisted of a preliminary rotation of East, North and Vertical (upward) component of ground motion according to a new reference system adapted to the slope surface geometry. The axes of the new reference are directed as the maximum slope direction (down-dip oriented), the slope strike direction (horizontal and normal to the previous one, oriented so to have the down-dip direction to the right) and the perpendicular to the slope surface (upward oriented).

For a slope inclined at a dip angle θ, and whose down-dip direction lies in a vertical plane forming an azimuth angle α with the local meridian plane, the transformation formulae are:

$$D(t) = E(t)\sin(\alpha)\cos(\theta) + N(t)\cos(\alpha)\cos(\theta) - U(t)\sin(\theta) \quad [1]$$

$$S(t) = -E(t)\cos(\alpha) + N(t)\sin(\alpha) \quad [2]$$

$$P(t) = E(t)\sin(\alpha)\sin(\theta) + N(t)\cos(\alpha)\sin(\theta) + U(t)\cos(\theta) \quad [3]$$

where $E(t)$, $N(t)$ and $U(t)$ are the East, North and Up components of the recorded ground motion and $D(t)$, $S(t)$ and $P(t)$ are the down-dip, strike and perpendicular components of ground motion in the new reference.

For the Mt. Dagang slope, the angles α and θ resulted to be about 100° and 40°, respectively. Figure 10 compares the results of the recordings of the first two measurement campaigns obtained from the analysis based on the new (rotated) reference system, and those obtained using the original (non-rotated) data. Overall, the diagrams derived from the rotated recordings appear less noisy and show more clearly the directional peaks of Rayleigh wave ellipticity. In fact, on an inclined surface, an analysis that estimates Rayleigh wave ellipticity from the ratio between horizontal and vertical components of ground motion is not able to optimize the cleaning of Rayleigh waves travelling along the slope surface from the contamination of other wave types. Therefore, the analysis of data acquired at the Mt. Dagang slope sites was subsequently carried out on rotated recordings.

4.3.1 Measurement outside the tunnels

Figure 11 reports the polar diagrams obtained from the HVIP analysis of data acquired at the free surface, just outside the L6 tunnel and at the entrance of the upper tunnel (site L7), whereas H/V curves along directions of maxima are shown in Fig. 12.

The first measurements acquired in October 2017 at L6 indicated the presence of a sharp peak (H/V=5.3) at 8.35 Hz, directed about orthogonally to the slope down-dip direction. The sharpness of this peak (Fig. 12a) raised the doubt about a possible artificial origin related to the roadworks carried out not far from the site. The measurements repeated one year later confirmed, however, the frequency and direction of the ellipticity peak maximum, with an even larger amplitude (H/V=6.7). Thus, such effect reflects a real site property, likely due to a strong directional resonance. Differently from other cases of site response directivity on slopes (e.g., Del Gaudio & Wasowski, 2011; Del Gaudio et al; 2018), the maximum of ground motion is not oriented along the maximum slope direction; this suggests a structural-geological control on site dynamic response rather than an effect of topography.

A recent study (Kleinbrod et al., 2019) proposed a classification of rock slope dynamic response to seismic shaking, distinguishing between depth- and volume-controlled responses. While the former type of site resonance is controlled by surface wave propagation through layers characterized by variations with depth of rock stiffness (e.g., as effect of weathering and/or diffuse fracturing), the response of the latter type depends on normal-mode vibrations affecting rock blocks separated by fracture systems. Volume-controlled response is typically characterised by sharper peaks in the ratios between horizontal and vertical component of ground motion, which are strongly polarized orthogonally to the fracture system. This seems the case of site L6, where slope materials are characterized by the presence of open fractures. At this site, the sharp polarized pattern of ratios between orthogonal directions of ground motion appears better revealed by the rotation of the reference system of ground motion recordings according to the slope surface inclination (see the two top-left polar diagrams in Fig. 10).

At the other site on Mt. Dagang slope, at the entrance of the L7 tunnel, our noise analysis indicated weaker site effects (Figs. 11, 12). The measurements carried out in June - October 2017 and October 2018 consistently showed a major resonance peak around 2 Hz, only slightly varying in frequency (1.95, 2.50 and 2.60 Hz for the three campaigns, respectively) and amplitude (3.8, 3.1 and 3.3, respectively), and possibly a secondary peak with amplitude less than 3 at frequencies between 6 and 8 Hz. Their direction angle (measured from the slope surface strike direction) varied only slightly between the two campaigns (between 55° and 75°), which confirms the directional nature of the site dynamic response. The resonance peaks directions are similar to the slope down-dip direction (E-W), differing by an angle between 15° and 35°.

With regard to the major peak, it is noteworthy that the results obtained as average over long recording sessions in October 2017 and October 2018 appear more similar to each other both in amplitude (3.1 – 3.3) and frequency (2.50 – 2.60 Hz) than in comparison to the outcome of the single measurement session carried out in June 2017. Thus, it is possible that the differences between the first campaign in June 2017 and the other campaigns reflect seasonal variations of slope material properties (e.g., water content variation before and after the rainfall season, respectively in June and October). Nevertheless, the amplitude of the Rayleigh wave ellipticity peak suggests that, differently from L6, the site amplification at L7 is not very high. Moreover, while the weaker resonance at L7 is close to down-dip direction, the stronger response at L6 is orthogonal.

4.3.2 Measurements at L7 inside the upper tunnel

A series of noise recordings was carried out next to the seven accelerometers of the array installed inside the upper water tunnel of Mt. Dagang, at the site L7 (Fig. 3d, e). These seismic stations were set up to investigate possible variations of site response inside tunnels, at different distances from the free surface.

Polar diagrams of HVIP values relative to the measurements acquired in the second (October 2017) and third campaign (October 2018) are shown in Fig. 13. In addition, Figure 14 compares HVIP curves derived from different measurement campaigns. The curves are arranged along significant directions, which do not necessarily coincide with the directions of maximum HVIP values. Indeed, at some stations, the largest peak in the measurements of one campaign appears along a direction different from that identified during the other campaigns. However, even in such cases, at least a secondary peak is present at frequency and direction consistent with those of the maxima of other measurements at the same site. The occasional presence of directional maxima, not confirmed by repeated measurements, was considered as a possible effect of transitory disturbance in noise wave field, not representative of site response properties.

Overall, the results obtained at different locations inside the tunnel did not show considerable variation of site response. The major peak (around 2 Hz) at site L7 at the tunnel entrance was also recognized at all the sites inside the tunnel, with a larger amplitude (between 3 and 5) than at L7 but similar orientation (55°-75° from the slope strike direction). The distinct secondary peak between 6

and 8 Hz present at the tunnel entrance was recognized only at the closest inner site (L7-1).
The only other peak consistently recurring at the same site was observed at the site L7-3, approximately halfway of the tunnel accelerometer array. Here a clear peak was observed in the three campaigns at similar frequencies (8.45, 8.40, 8.30 Hz,), with amplitude almost identical in the first two campaigns (3.6 and 3.7, respectively) and a bit larger (4.5) in the last one, with consistent orientation close to that of slope surface strike (165°-175°). Such an effect could be related to local geological features (e.g., rock fracturing). However, the presence of the tunnel lining did not allow us to obtain information about the rock mass structure.
One could expect a reduction of the site amplification factor toward the innermost measurement points in the tunnel, as effect of the increase of distance from the free surface where direct and reflected waves overlap with constructive interference. However, the amplitude of the ~2 Hz peak did not show a significant decrease between L7-1 and L7-7. This could be due to the limited length of the seismic array (~240 m), which is likely insufficient to appreciate the expected decrease of amplification with depth. Indeed, assuming high velocities of the moderately to slightly weathered granite formation, one can expect that longer (then the tunnel) wavelengths characterize seismic waves at the relatively low frequency of the resonance peak .

5. Discussion

Some of the accelerometer stations in the Lengzhuguan area had recorded three seismic events, i.e., the Ms 7.0 mainshock of the 2013 Lushan earthquake, at epicentral distance of 85 km, and the two major shocks (Ms 6.3 and 5.8) of the 2014 Kangding sequence, at distances of 40-50 km, to the ENE (Lushan) and WNW (Kangding) of Lengzhuguan (Fig. 1). Even though the number of recorded events is small for a robust analysis of site response properties, it is possible to evaluate the consistency of the earthquake data with the outcome of our ambient noise analysis.
Seismic recordings were analysed using the HVSR technique (Lermo and Chávez-García, 1993), which follows the same approach used by Nakamura (1989) for noise analysis, i.e., the calculation of spectral amplitudes between horizontal and vertical components of recordings, averaged over several events. Figure 15 reports the results of the analysis for the sites that recorded the mentioned earthquakes.
At sites L1 and L2 (Fig. 15a-b), there is evidence of very strong resonance with a NE directed maximum at 2.0 Hz. Furthermore, we identified secondary SE directed peaks at 3.0 and 2.4 Hz at L1 and L2, respectively, and an additional peak in approximately E-W direction at 1.2 Hz at L2. In

relative terms, the amplification appears considerably stronger at the top of the hill (L1) for higher frequencies (between 2 and 4 Hz).

Overall, these results are consistent with those derived from ambient noise analysis, demonstrating that the Mt. Huoshao exhibits a complex pattern of dynamic response including differently directed resonance peaks at frequencies between 2 and 4 Hz. Each of these peaks appears more or less pronounced in the different parts of the relief, with large amplitude values at the mid-slope site L2 (at a frequency close to 2 Hz), as well as at the top of the hill, but at higher frequencies. The 2.0 Hz component of the site effect present at both the top and at mid-slope of the hill, is likely to act at the scale of the entire hillslope.

The results derived from the analysis of L5 accelerograms (Fig. 15c) indicate a major resonance effect at a frequency of 4.5 Hz, quite similar to that shown by HVIP noise analysis at around 5 Hz. However, the spectral ratio maximum is not very pronounced (H/V=3.4). The directions of HVSR maxima differ from the results of noise analysis, being rotated towards an EW orientation. This suggests the absence of a clear site-specific directivity in site dynamic response.

With regard to the sites on the sub-planar slope of Mt. Dagang, for the sites L7 and L7-6 (Fig. 15e-f), HVSR results are in agreement with the outcomes of our noise analysis, confirming a weak-moderate amplification effect at a frequency close to 2 Hz along a direction subparallel to that of maximum slope. Conversely, at L6 (Fig. 15d), the HVSR results from the seismic data show no evidence of the strong slope-strike-directed resonance at ~8 Hz revealed by the HVIP analysis. However, the few available seismic recordings had major energy content concentrated on relatively low frequencies, as effect of relatively large magnitudes and long epicentral distances. Therefore, they probably did not have enough energy at the frequencies of L6 resonance (8 Hz).

Overall, the dynamic response results from the combined noise and seismic data indicate that the slopes potentially most susceptible to be destabilized by earthquake shaking are those around the confluence of the Lengzhuguan Torrent to the Dadu River. Here one can expect strong amplification effects at frequencies low enough (2-5 Hz) to trigger large mass movements. Future seismically induced slope failures represent a threat for the Lengzhuguan village and the road running along the Dadu River. Furthermore, slope failures could cause the damming of the torrent with additional problems of public safety.

The effects of site amplification appear less critical for the seismic stability of the long sub-planar slope of Mt Dagang facing the Dadu River, at least as regards its mid-low portion investigated in this study. Indeed, significant amplifications have a strong directivity transversal to the maximum slope direction and affect only higher frequencies (~ 8 Hz). This imply destabilizing influence on smaller volume rock masses. Furthermore, where lower frequency resonances were identified along directions close to maximum slope, they appear characterized by a lower amplification factor.

.

6. Conclusions

The outcomes of this study offered insights on the potential of combining ambient noise analysis with data derived from accelerometer monitoring of steep slopes subject to seismically induced failures. This is particularly relevant in situations where the accelerometer monitoring have provided only a limited amount of recordings. For the selected slope sites around the village of Lengzhuguan, we took advantage of the new analysis technique (HVIP), which allows isolating Rayleigh waves inside noise recording, and measuring properties of these waves that reflect site response characteristics. The technique, based on the identification of instantaneous polarization properties, proved to be applicable also to long steep slopes, by rotating the three-component noise records according to a reference adapted to the slope surface geometry. This allowed us to recognize more clearly the ellipticity of Rayleigh waves travelling along steeply inclined surfaces.

The important information derived from the advanced ambient noise analysis, backed by the good consistency with the available accelerometer monitoring data, is that significant site amplification effects can occur on slopes around the confluence of the Lengzhuguan torrent with the Dadu River. This is related to the presence of surficial deposits overlying the intensely fractured granite bedrock, which make the slope materials more prone to be mobilized (or remobilized) by future earthquakes.

The analysis of the site response along the middle-lower part of the Mt. Dagang slope facing the Dadu River indicates lower susceptibility to the destabilizing effect of seismic shaking. Site amplification is locally present, but appears characterized by resonance effect with frequency, amplitude or direction that do not facilitate the occurrence of large slope failures.

Finally, the analysis of site dynamic response inside the slope, based on ambient noise recording within a 240 m long tunnel, did not point out significant variations in site response properties between the entrance and the end of the tunnel. This is possibly due to the circumstance that, the array of the measurement points is not long enough with respect to the wavelengths involved in resonance effects to allow distinguishing the variations expected when moving from the free surface to the inner part of the slope.

Acknowledgements

Study sponsored by the Chengdu University of Technology (P.R. China) through the Open Fund of the State Key Laboratory of Geohazard Prevention and Geoenvironment Protection with Project No. SKLGP2017K004. We also thank prof. Huang Runqiu for encouraging the long-term investigations on seismic susceptibility of slopes to failure in Sichuan. Insightful comments by an anonymous reviewer helped us to improve the original manuscript.

References

Allen, C.R., Luo, Z., Qian, H., Wen, X., Zhou, H., Huang,, W., 1991. Field study of a highly active fault zone: the Xianshuihe fault of southwestern China. Geol. Soc. Am. Bull., 103, 1178–1199.

Bard, P.Y. and the SESAME Team, 2004. Guidelines for the implementation of the H/V spectral ratio technique on ambient vibrations. SESAME European research project WP12 – Deliverable D23.12, 62 pp, ftp://ftp.geo.uib.no/pub/seismo/SOFTWARE/SESAME/USER-GUIDELINES/SESAME-HV-User-Guidelines.pdf.

Bonnefoy-Claudet, S., Cotton, F., Bard, P.-Y., 2006. The nature of seismic noise wavefield and its implications for site effects studies – A literature review, Earth-Sci. Rev., 79, 205–227.

Burjánek, J., Edwards, B., Donat Fäh, D., 2014. Empirical evidence of local seismic effects at sites with pronounced topography: a systematic approach. Geophysical Journal International. 197, Issue 1, 608–619.

Burjánek, J., Gischig,V., Moore, J.R., Donat Fäh, D., 2018. Geophys. J. Int. 2018. Ambient vibration characterization and monitoring of a rock slope close to collapse. 212, 297–310.

Chen, X. L., Zhou, Q., Ran, H., Dong. R., 2012. Earthquake-triggered landslides in southwest China. Nat. Hazards Earth Syst. Sci., 12, 351–363.

China Earthquake Database (CENC), http://www.ceic.ac.cn/history (last accessed 14 May, 2018).

Dai, F.C., Leeb, C.F., Deng, J.H., Tham, L.G. 2005. The 1786 earthquake-triggered landslide dam and subsequent dam-break flood on the Dadu River, southwestern China. Geomorphology. 65, 205–221.

Deng H., Wu L.Z., Huang R.Q., Guo X.G., He Q. 2017. Formation of the Siwanli ancient landslide in the Dadu River, China. Landslides, 14, 385-394.

Del Gaudio, V., 2017. Instantaneous polarization analysis of ambient noise recordings in site response investigations. Geophys. J. Int., 210, 443–464, doi: 10.1093/gji/ggx175.

Del Gaudio, V., Wasowski, J., 2011. Advances and problems in understanding the seismic response of potentially unstable slopes. Eng. Geol. 122, 73–83.

Del Gaudio, V., Muscillo, S., Wasowski, J., 2014. What we can learn about slope response to earthquakes from ambient noise analysis: An overview. Eng. Geol., 182, 182-200.

Del Gaudio, V., Luo, Y., Wang, Y., Wasowski J., 2018. Using ambient noise to characterise seismic slope response: the case of Qiaozhuang peri-urban hillslopes (Sichuan, China). Eng. Geol., 246, 374-390, doi: 10.1016/j.enggeo.2018.10.008.

Fan X.M., Juang, CH, Wasowski, J., Huang, R.H., Xu, Q., Scaringi, G., van Westen, C.J., Havenith, H-B. 2018. What we have learned from the 2008 Wenchuan Earthquake and its aftermath: A decade of research and challenges. Eng. Geol., 241, 25-32.

Fei, C., Deng, J., Gao, M., Wang, D., Meng, Y., Huang, RQ., 2012. Geological cause and stability evaluation of Moluocun landslide, Danba County. Rock Soil Mech. 33 (6), 1781–1786.

Harp, E.L., Noble, M.A., 1993. An engineering rock classification to evaluate seismic rock-fall susceptibility and its application to the Wasatch Front. Bull. Assoc. Eng. Geol. 30 (3), 293–319.

Keefer, D., 1993. The susceptibility of rock slopes to earthquake-induced failure. Bull. Assoc. Eng. Geol. 30 (3), 353–361.

Kleinbrod, U., Burjánek, J., Fäh, D. 2019. Ambient vibration classification of unstable rock slopes: A systematic approach. Engineering Geology, 249, 198-217. doi: 10.1016/j.enggeo.2018.12.012

Lermo, J., Chávez-García, F.J., 1993. Site effect evaluation using spectral ratios with only one station. Bull. Seism. Soc. Am., 83, 1574-1594.

Luo YH, Wang YS, He Yuan, et al. (2013) Monitoring result analysis of Lengzhuguan slope ground shock response of Lushan earthquake of Sichuan, China. Journal of Chengdu University of Technology (Science &Technology Edition) 40(3):232-241. (in Chinese).

Luo, Y., Del Gaudio, V., Huang, R., Wang, Y., Wasowski, J., 2014. Evidence of hillslope directional amplification from accelerometer recordings at Qiaozhuang (Sichuan — China). Eng. Geol., 183, 193-207, doi:10.1016/j.enggeo.2014.10.015.

Moore, J.R., Gischig, V., Burjanek, J., Loew, S., Fäh, D., 2011. Site Effects in Unstable Rock Slopes: Dynamic Behavior of the Randa Instability (Switzerland). Bull. Seism. Soc. Am. 101 (6), 3110–3116.

Morozov, I. B., Smithson, S. B., 1996. Instantaneous polarization attributes and directional filtering, Geophysics, 61, 872-881.

Nakamura, Y., 1989. A method for dynamic characteristics estimation of subsurface using microtremor on the ground surface. Q. Report Railway Tech. Res. Inst., 30, 25–33.

Tu, Y.J., Linghu, KH., Wang, Y. 2018. Exploration and practice of hierarchical management and control system construction of dangerous sites in the Dadu River basin. Water Power, 44(5), 77-11 (In Chinese with English abstract).

Wang YS, He JX, Luo YH, 2015. Seismic monitoring of a slope to investigate topographic amplification. International Journal of Geohazards and Environment, 1(3): 101-109.

Wang YS, He JX, Luo YH. 2017. Seismic response of the Lengzhuguan slope during Kangding Ms5.8 earthquake. J. Mt. Sci. 14(11): 2337-2347.

Wasowski, J., Lee, C.T., Keefer, D., 2011. Toward the next generation of research on earthquake induced landslides: Current issues and future challenges. Eng. Geol., 122, 1–8, doi:10.1016/j.enggeo.2011.06.001.

Wathelet, M, 2008. An improved neighbourhood algorithm: parameter conditions and dynamic scaling. Geophys. Res. Lett., 35, L09301, doi:10.1029/2008GL033256.

Xu, G.Q., Kamp, P.J.J. 2000. Tectonics and denudation adjacent to the Xianshuihe Fault, eastern Tibet Plateau: Constraints from fission track thermochronology. J. Geoph. Res., 105, No. B8, 19231-19251.

Figures

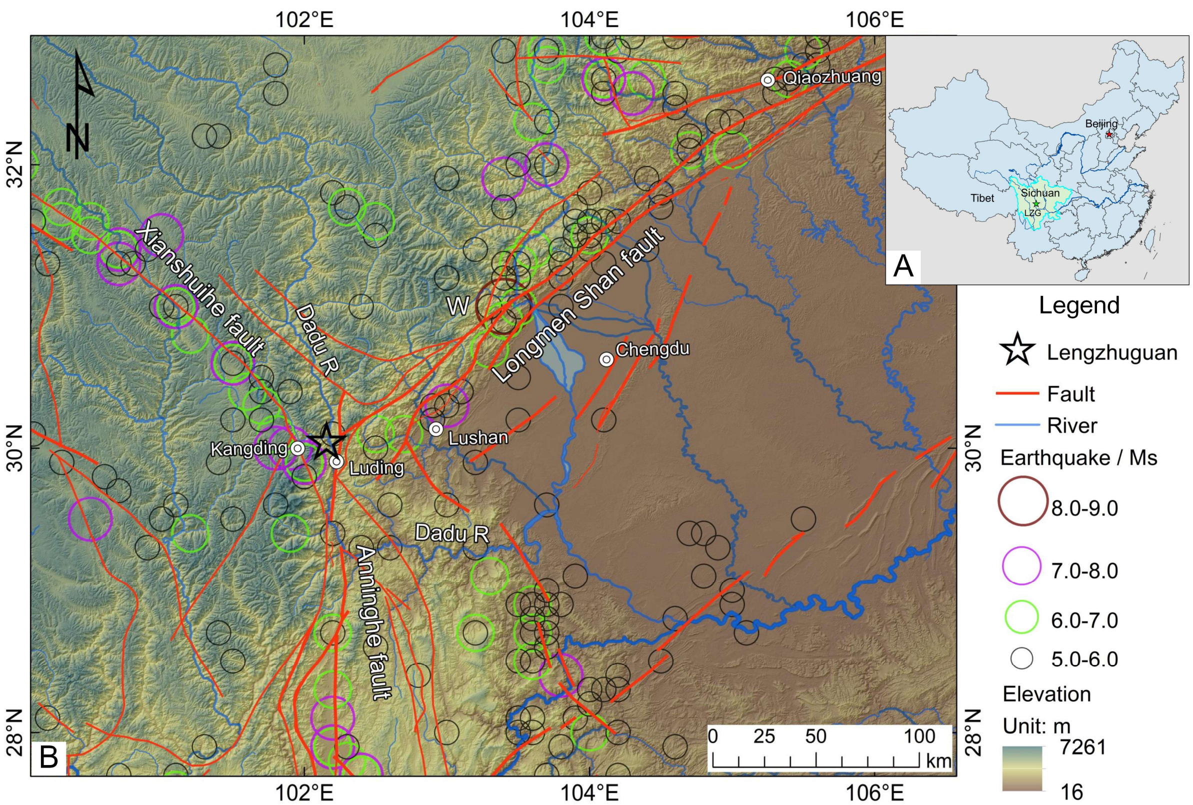

Fig. 1 Regional setting and location of the Lengzhuguan study area in Sichuan Province (inset A). W – epicenter of the 2008 Mw 7.9 Wenchuan earthquake. Earthquake and fault data from the China Earthquake Database (CENC), http://www.ceic.ac.cn/history.

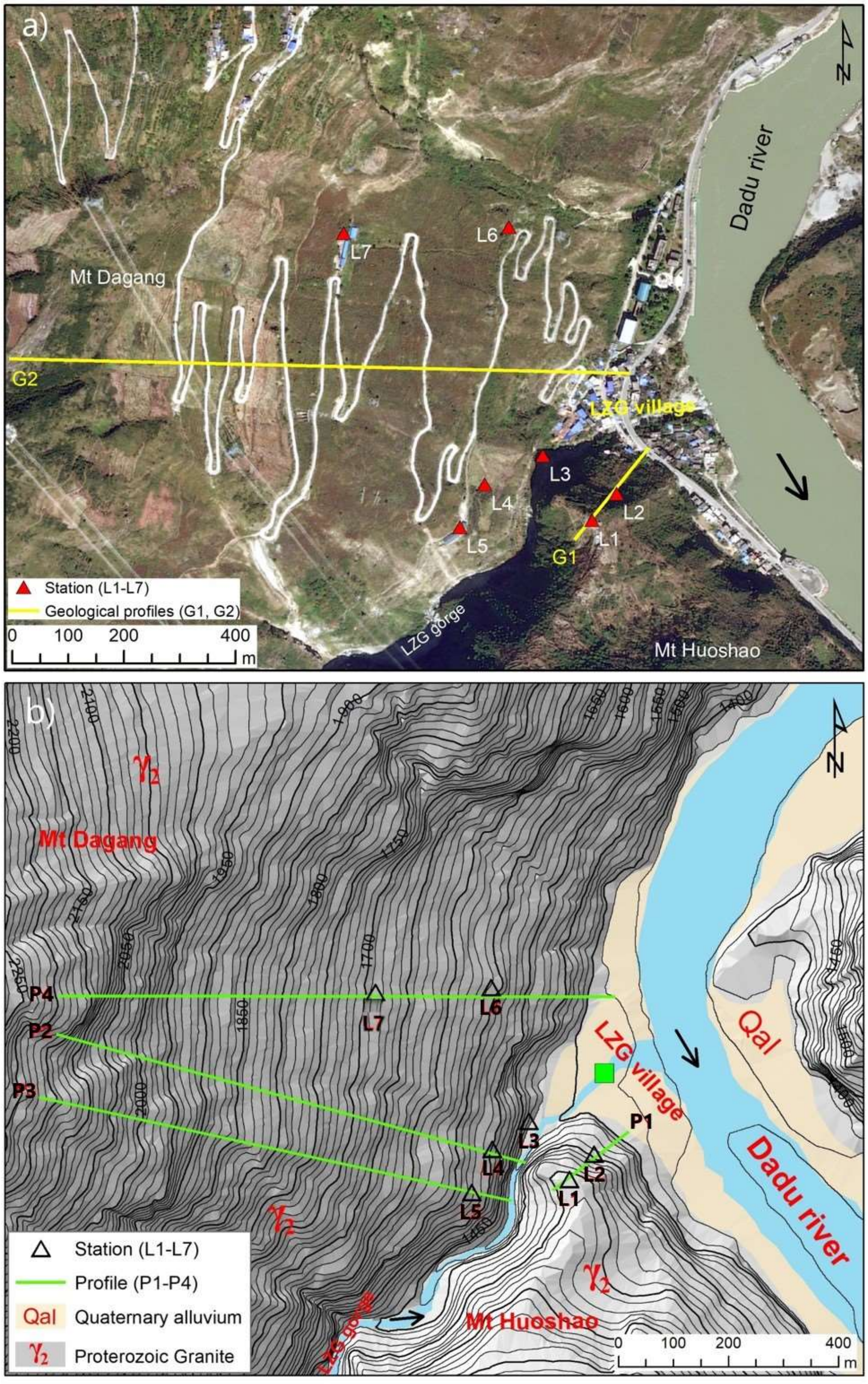

Fig. 2 a) Aerial view of the Lengzhuguan (LGZ) study area on the west valley side of the Dadu River; L1-L7 sites of accelerometer stations and ambient noise recordings; G1-G2 location of geological sections shown in Fig. 4. b) Topographic and lithologic features of the study area. P1-P4 locations of topographic profiles shown in Fig. 3.

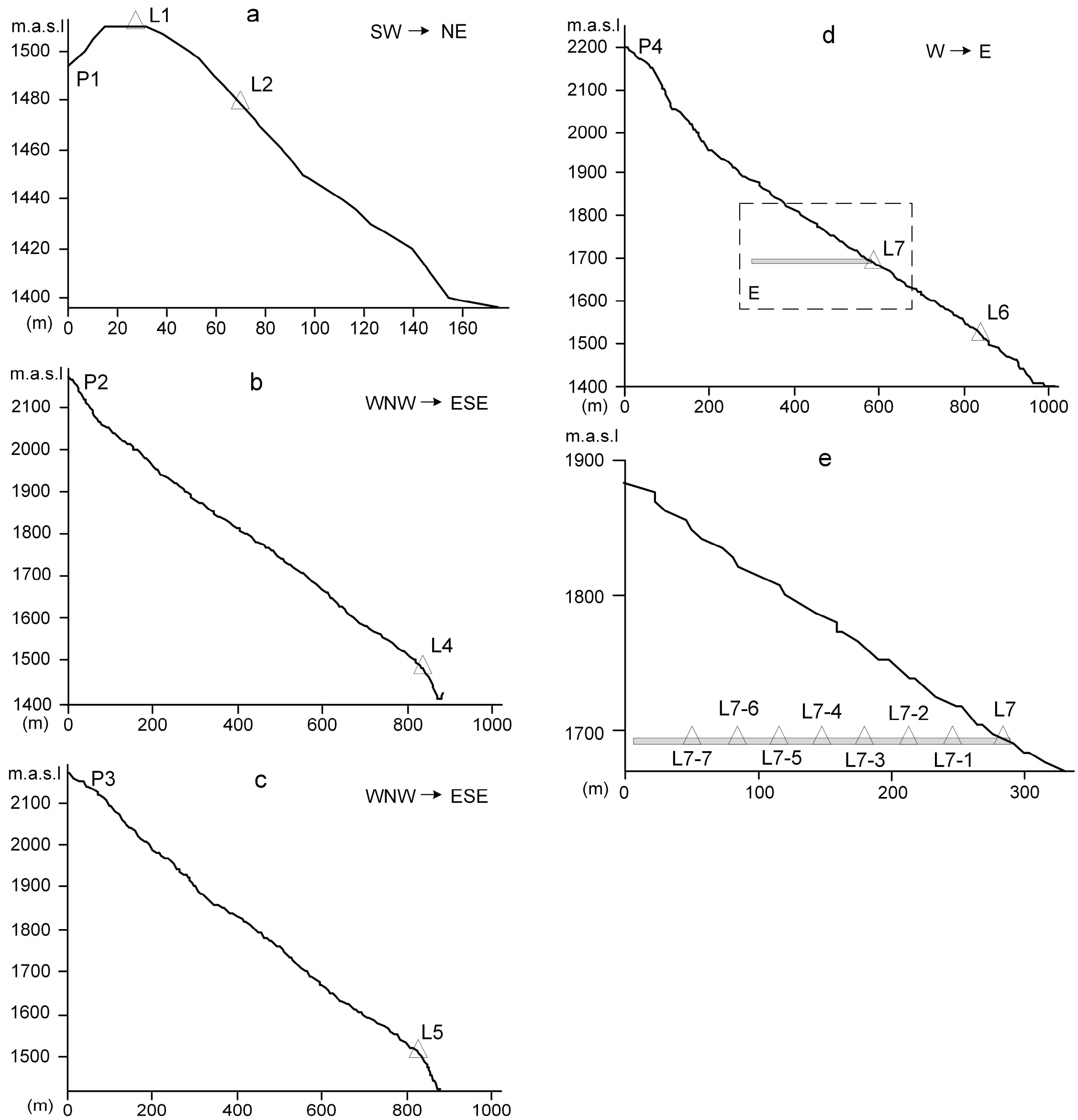

Fig. 3 Topographic profiles of the Mt. Huoshao (P1) and Mt. Dagang (P2, P3, P4) slopes at locations indicated in Fig. 2b. L1-L2-L4 and L5 and, in Figure 3-e, L7, L7-1, L7-2, L7-3, L7-4, L7-5, L7-6 and L7-7, are sites of accelerometer stations and ambient noise recordings. Note several stations located inside the rocky slope in an abandoned water tunnel (Fig. 3-e).

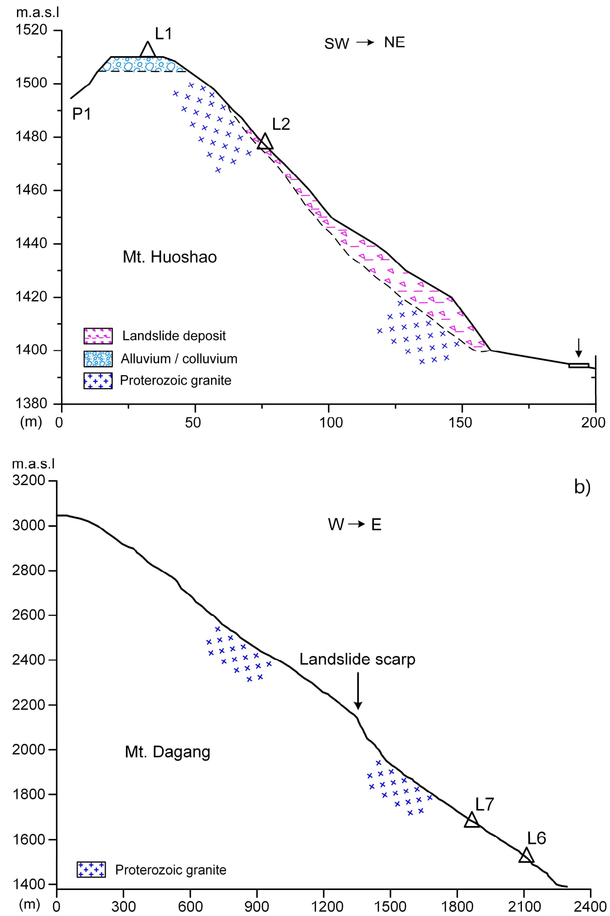

Fig. 4 Geological cross-sections: G1 of Mt Huoshao (a) and G2 of Mt Dagang (b). See Fig. 2a for location.

Fig. 5 View of the Mt Dagang slope facing the Dadu River and the Lengzhuguan village (photo by J. Wasowski). Red triangles mark the locations of stations L6 and L7 at the entrance of two water tunnels. Note about 100 m high slope break interpreted as scarp of an old landslide.

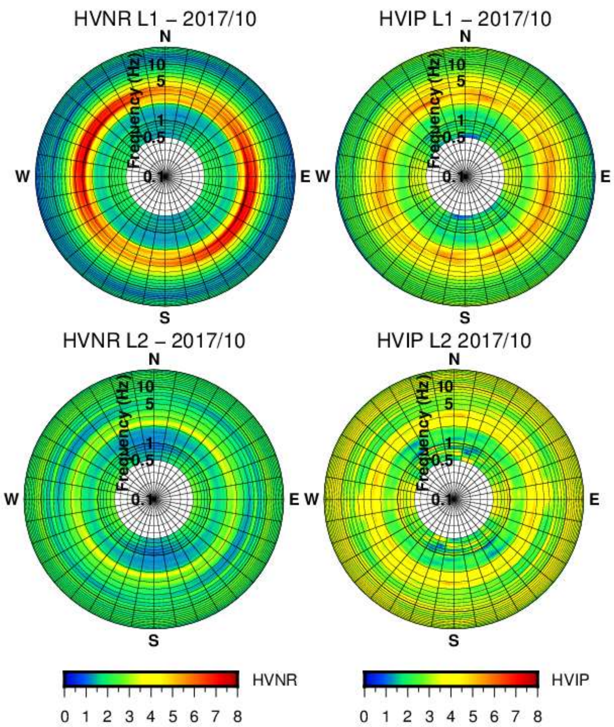

Fig. 6: Polar diagrams of HVNR (spectral ratios values) and HVIP (Rayleigh wave ellipticity) for sites L1 and L2, on the top and at mid-slope, respectively, of Mt. Huoshao (see Fig. 2 for location); results based on the measurements acquired in October 2017. Colour scale provides the value of H/V ratio (between horizontal and vertical component of ground motion) as function of frequency (radially plotted) along different directions.

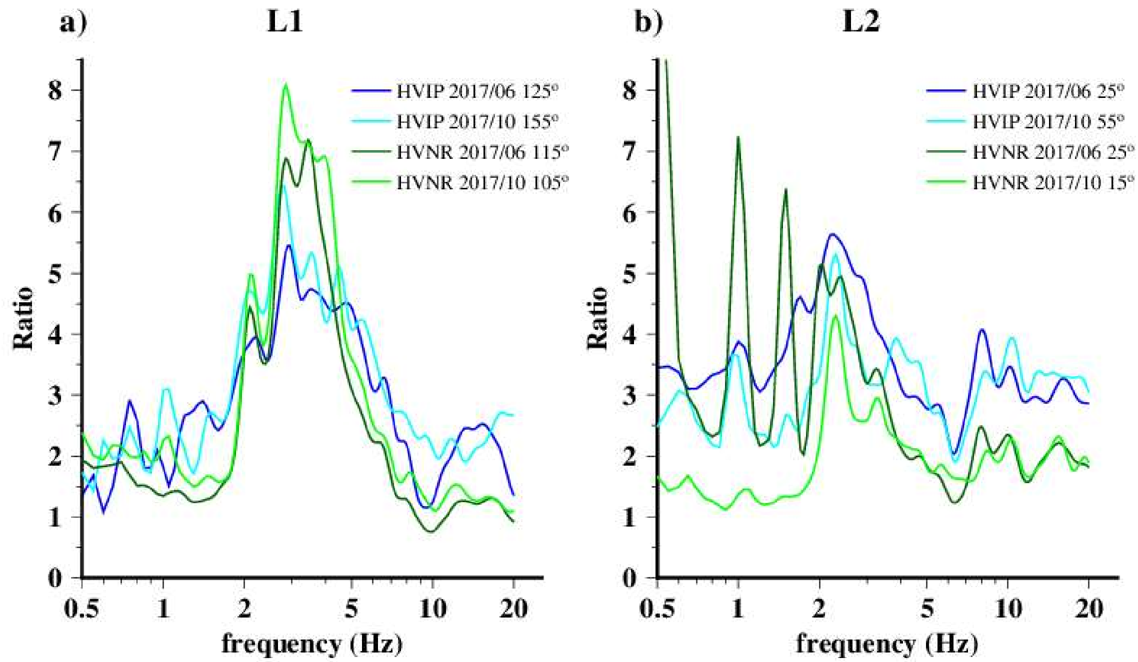

Fig. 7: Comparison of curves of HVNR and HVIP values obtained at sites L1 (a) and L2 (b) along directions of peak values (azimuths specified in legend), from the measurements carried out in June and October 2017.

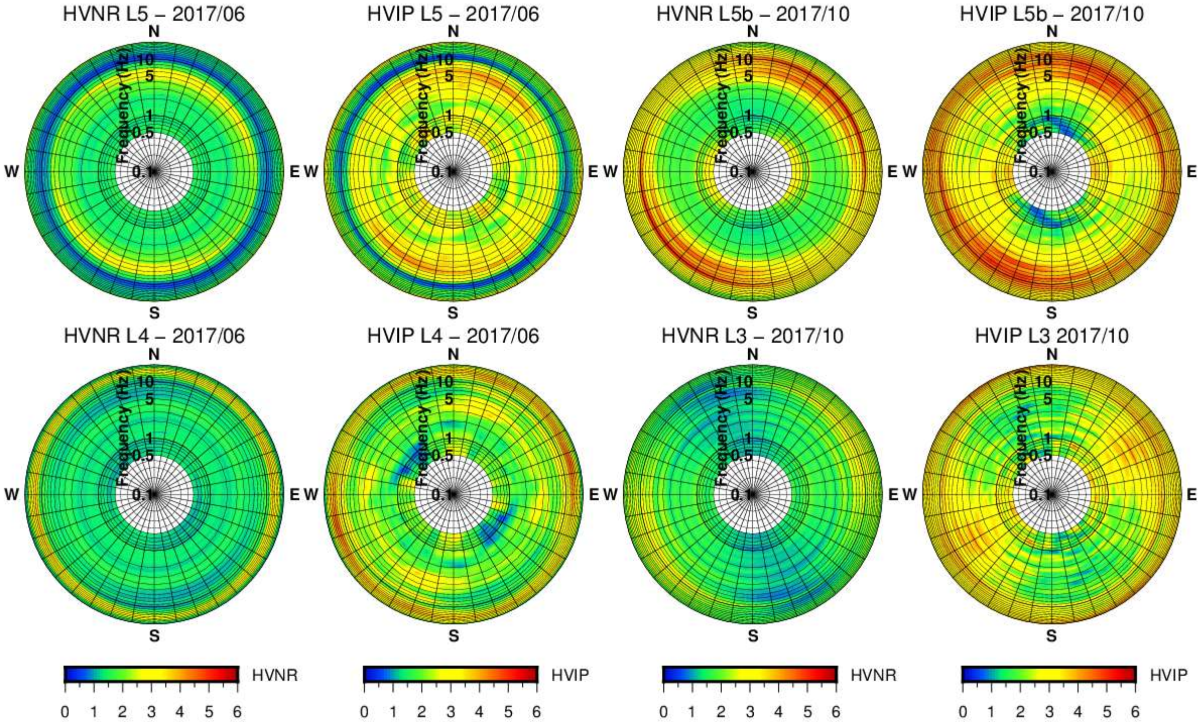

Fig. 8: Polar diagrams of HVNR and HVIP for sites L3, L4, L5 and L5b, at lower part of Mount Dagang slope, NW side of the Lengzhuguan torrent (see Fig. 2 for location); results based on measurements acquired in June and October 2017. Colour scale provides the value of H/V ratio as function of frequency along different directions.

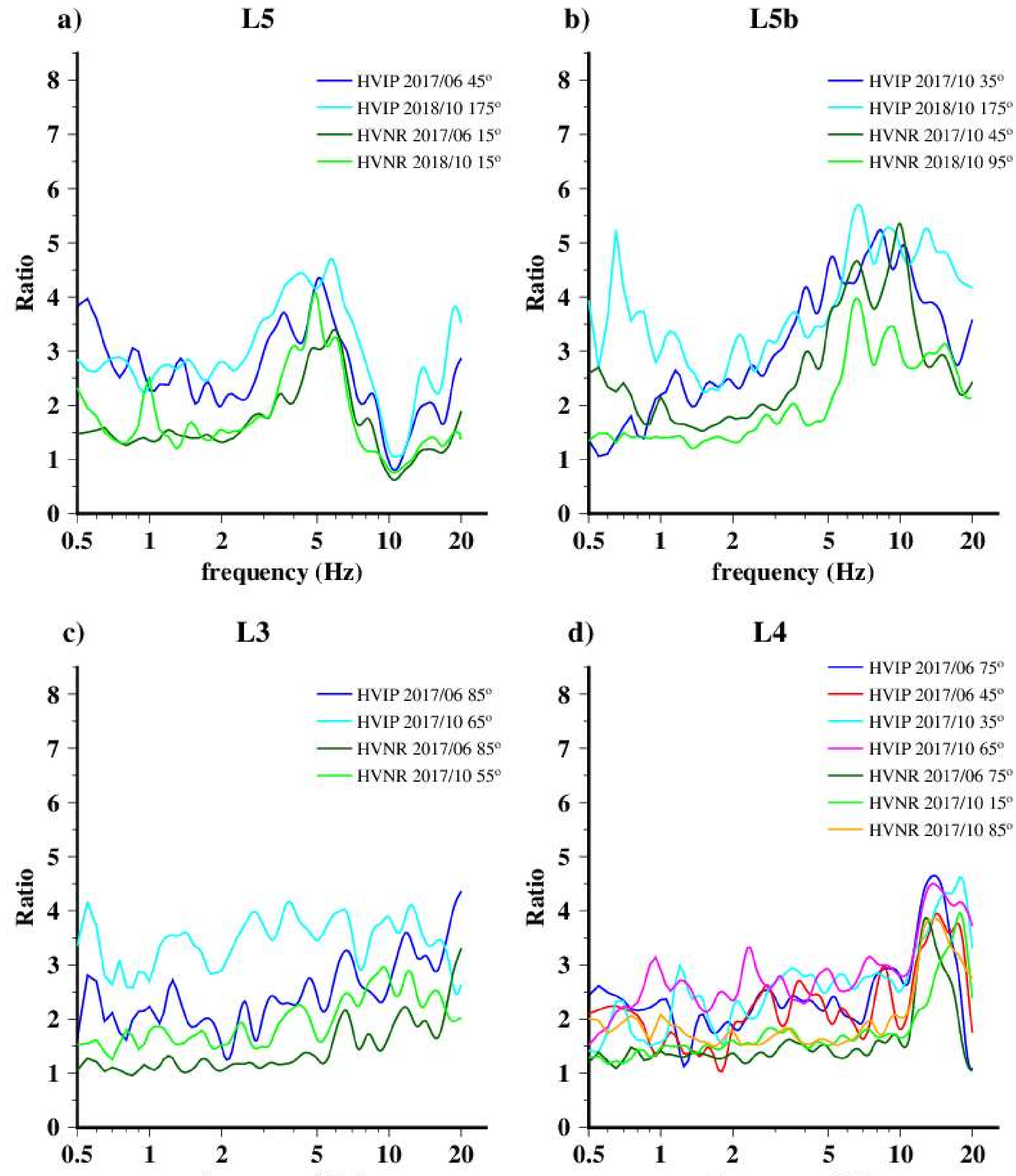

Fig. 9: Comparison of curves of HVNR and HVIP values obtained at sites L5 (a), L5b (b), L3 (c) and L4 (d) along directions of peak values (azimuths specified in Legend), based on the measurements carried out in June and October 2017 and in October 2018.

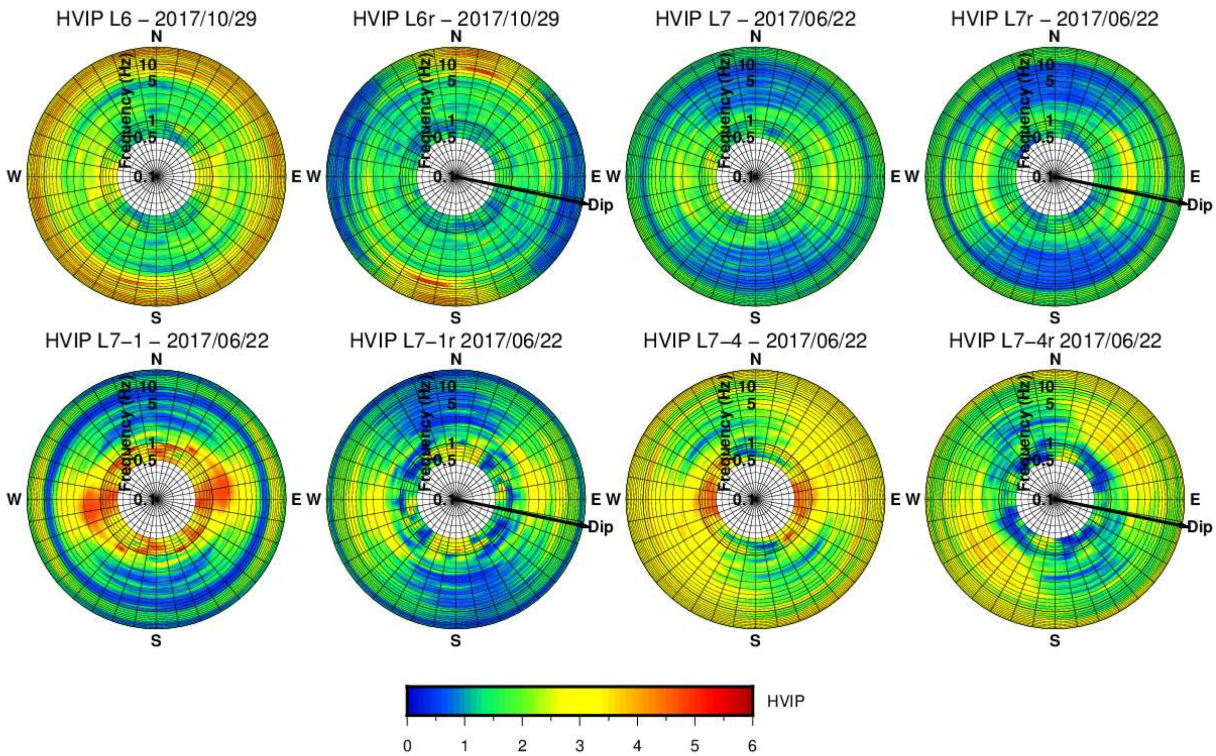

Fig. 10: Comparison of the results obtained from the HVIP analysis applied to the original recordings (with components East, North and Up) and the rotated recordings (with components Down-dip, Strike and Perpendicular) at Mt. Dagang sites L6 and L7 (see Fig. 2 for location); suffix r added to the site name marks the results based on the rotated recordings). Black arrows indicate the azimuth of slope down-dip direction.

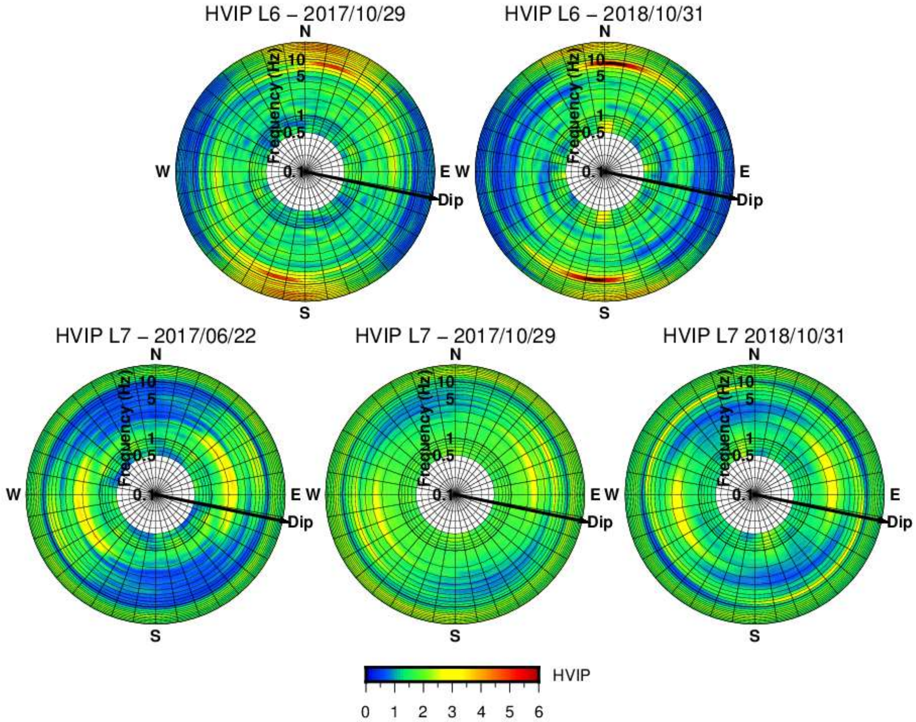

Fig. 11: Polar diagrams of HVIP for sites L6 and L7, on the sub-planar slope of Mt. Dagang sites (see Fig. 2 for location). Results based on measurements acquired in three different periods (June and October 2017, October 2018). Colour scale provides the value of Rayleigh wave ellipticity as function of frequency along different directions.

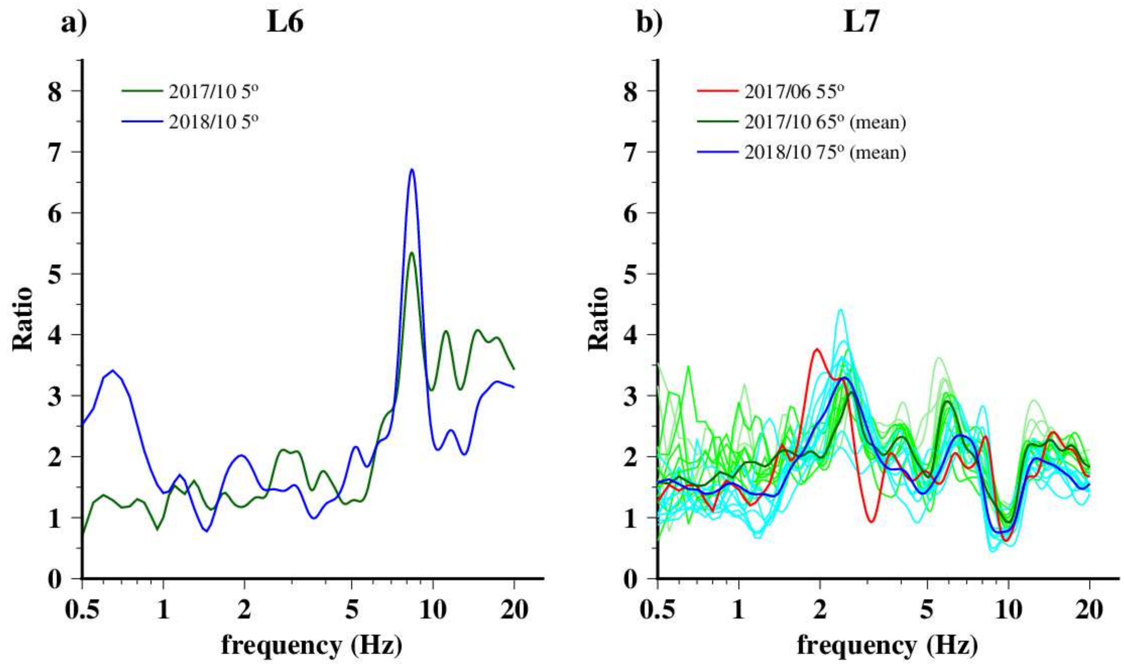

Fig. 12: Curves of HVIP values, along peak value directions, obtained for sites L6 (a) and L7 (b) from different measurement campaigns, as specified in Legend. Note that direction angles are calculated clockwise from the strike direction of slope surface. For L7 site data based on very long measurement sessions in October 2017 and 2018, lighter colour curves (blue and green) represent the results obtained from half an hour recording intervals, whereas the darker curves are relative to the averages.

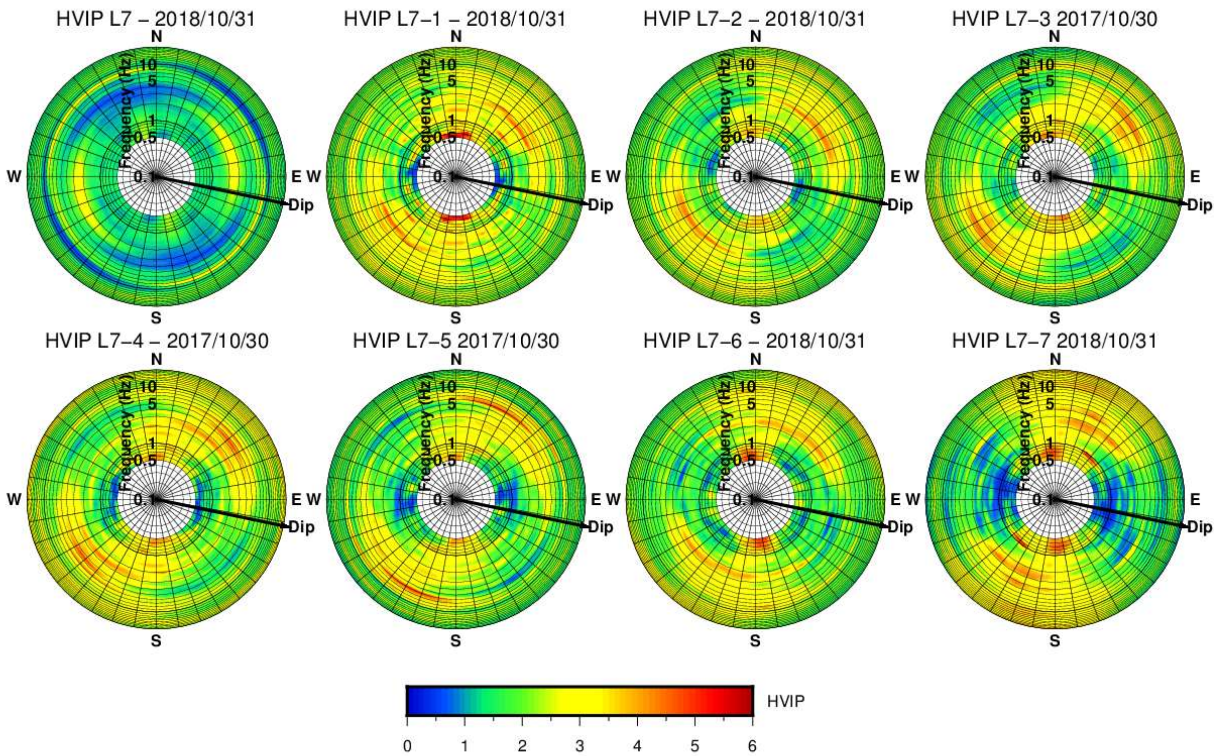

Fig. 13: Polar diagrams of HVIP for sites inside the L7 tunnel (see Figs. 2 and 3d, e for location). Colour scale provides the value of Rayleigh wave ellipticity as function of frequency along different directions.

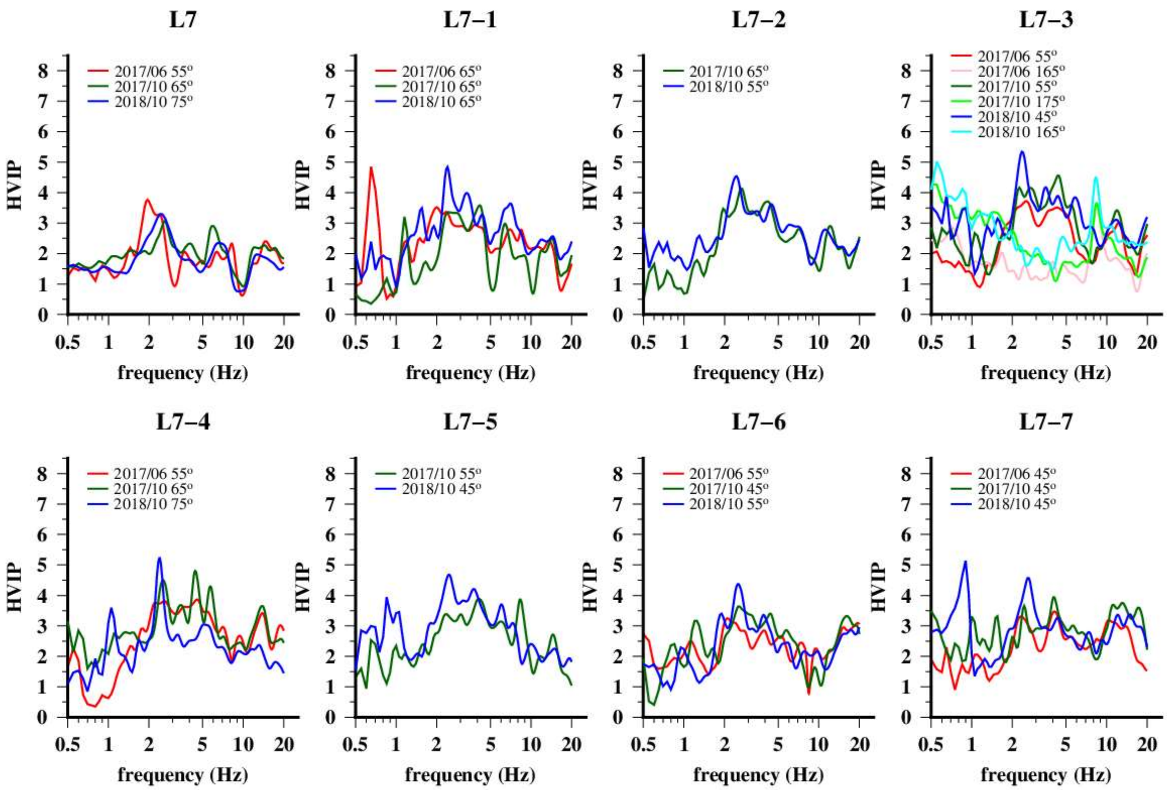

Fig. 14: Curves of HVIP values obtained at the sites of the accelerometer stations located inside the upper tunnel of Mt. Dagang (see Figs. 2 and 3d, e for location). Legends report the dates and angular directions calculated clockwise from the slope surface strike for curves obtained from different measurement campaigns.

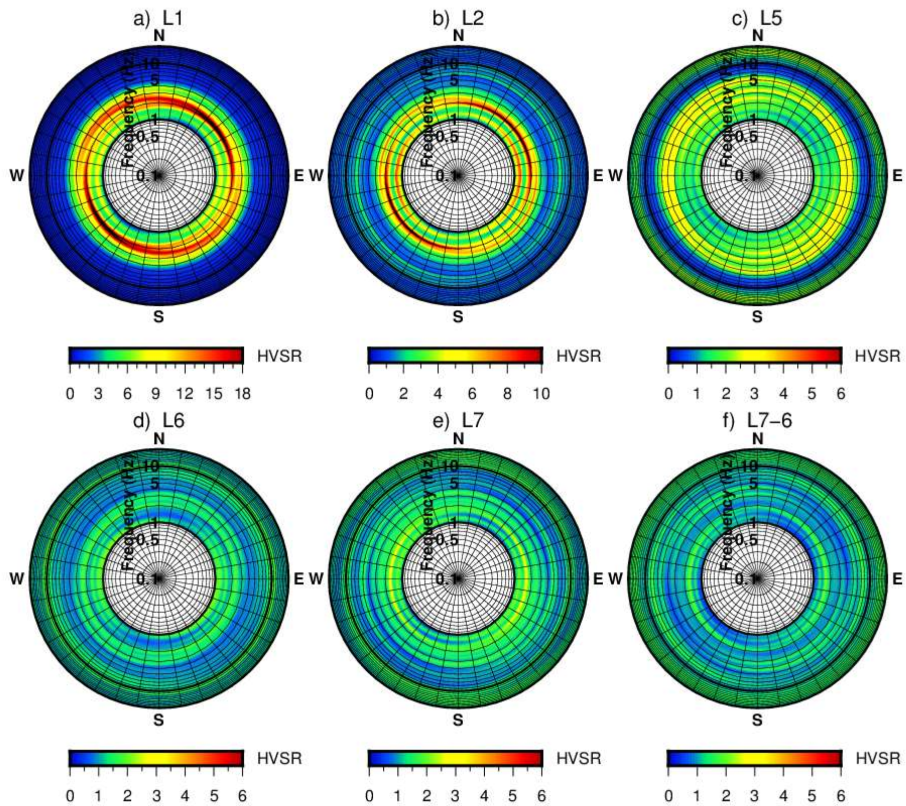

Fig. 15: Polar diagrams of the results of the HVSR analysis of accelerometer recordings for sites L1, L2, L5, L6, L7 and L7-6 (see Fig. 2 for location).